npj Precision Oncology

https://doi.org/10.1038/s41698-025-01206-y

Article in Press

Deciphering brain metastasis in epithelial ovarian cancer: multimodal analysis and potential biomarkers

Received: 29 April 2025

Accepted: 17 November 2025

Cite this article as: Trozzi, R., Salvi, M., Karimi, M. *et al.* Deciphering brain metastasis in epithelial ovarian cancer: multimodal analysis and potential biomarkers. *npj Precis. Onc.* (2026). https://doi.org/10.1038/s41698-025-01206-y

R. Trozzi, M. Salvi, M. Karimi, A. Minucci, G. Raspaglio, M. De Donato, M. Buttarelli, A. Piermattei, L. Vaccaro, A. Grimaldi, R. De Santis, M. Massa, F. Sillano, L. Giacò, L. Mastrantoni, V. Iacobelli, F. Camarda, M. Cesana, S. Duranti, M. C. Sassu, P. Mattogno, A. Fagotti, C. Marchetti, G. Scambia, C. Nero & D. Cacchiarelli

Deciphering Brain Metastasis in Epithelial Ovarian Cancer: Multimodal analysis and Potential Biomarkers.

Authors

Trozzi R.*[1,2], Salvi M.*[3,4], Karimi M.[5], Minucci A.[6,7], Raspaglio G.[6,7], De Donato M.[6,7], Buttarelli M.[7], Piermattei A.[1], Vaccaro L[3,4]., Grimaldi A.[3,4,8], De Santis R.[3,4], Massa M.[3,4], Sillano F.[1], Giacò L.[5], Mastrantoni L.[9], Iacobelli V.[1,2], Camarda F.[1,2], Cesana M.[3,8], Duranti S.[10], Sassu M. C.[1,2], Mattogno P.[11], Fagotti A.[1,7], Marchetti C.[1,7], Scambia G.[1,7], Nero C. ±[1,7], Cacchiarelli D. ±[3,4,8]

* Co-first

± Co-last

Affiliations

1 Department of Women's, Children's and Public Health Sciences, Fondazione Policlinico Universitario A. Gemelli, IRCCS, Rome, Italy

2 Catholic University of the Sacred Heart, Rome, Italy

3 Telethon Institute of Genetics and Medicine (TIGEM), Armenise/Harvard Laboratory of Integrative Genomics, Pozzuoli, Italy

4 Department of Translational Medicine, University of Naples "Federico II", Naples, Italy

5 Bioinformatics Research Core Facility, Gemelli Science and Technology Park (GSTeP), Fondazione Policlinico Universitario A. Gemelli IRCCS, Rome, Italy

6 Departmental Unit of Molecular and Genomic Diagnostics, Fondazione Policlinico Universitario A. Gemelli IRCCS, Rome, Italy

7 University Department of Life Sciences and Public Health, Section of Gynecology and Obstetrics, Catholic University of the Sacred Heart, Rome, Italy

8 Genomics and Experimental Medicine Program, Scuola Superiore Meridionale (SSM, School of Advanced Studies), Naples, Italy

9 Medical Oncology, Università Cattolica del Sacro Cuore, Rome, Italy

10 Scientific Directorate, Fondazione Policlinico Universitario A. Gemelli, IRCCS, Rome, Italy

11 Department of Neurosurgery, Fondazione Policlinico Universitario A. Gemelli IRCCS, Rome, Italy

Contact information

Fagotti Anna, MD., PhD anna.fagotti@policlinicogemelli.it

Abstract

Epithelial ovarian cancer (EOC) remains the most lethal gynaecological malignancy in developed countries, with recurrence and drug resistance posing significant clinical challenges. Brain metastases (BM) from epithelial ovarian cancer, once rare, are an increasing phenomenon and are characterised by a dismal prognosis. To explore the molecular underpinnings of BM in EOC, we conducted a multimodal genomics and transcriptomics analysis of matched primary tumour and brain metastases samples from a retrospective cohort. Our findings revealed high genomic concordance between primary tumour (PT) and BM, with alterations in key pathways such as *MYC* (MYC Proto-Oncogene, bHLH Transcription Factor) targets, extracellular matrix remodelling, and inflammatory signalling characterizing the BM. *AFP* (Alpha-fetoprotein) and *GFAP* (Glial Fibrillary Acidic Protein) emerged as potential biomarkers from the primary lesion for BM onset, while network analysis identified *MET* (MET Proto-Oncogene, Receptor Tyrosine Kinase), *GDF15* (Growth Differentiation Factor 15), and *S100A9* (S100 Calcium Binding Protein A9) as candidate mediators of tumor-brain crosstalk. These results offer new insights into EOC brain tropism, highlighting potential targets for therapeutic intervention and personalized patient management in the precision oncology era.

Introduction

Epithelial ovarian cancer (EOC) is the deadliest gynaecological malignancy in developed countries. Despite the improvement in the therapeutic strategies, around 80% of patients experience recurrence and ultimately develop drug resistance. The recurrences are frequently confined to the abdominal cavity, where the peritoneum is the most common involved site. Only 8% of the recurrent patients show isolated distant metastases without concomitant peritoneal or nodal disease[1]. Brain metastases (BM) from EOC are late-stage, uncommon disease manifestations usually occurring in the context of a widely disseminated disease. The reported incidence of BM in EOC patients ranges from 0.3 to 11% in different series[2–3–4]. However, the incidence of BM is expected to rise in the coming years due to extended survival conferred by targeted therapies, such as poly (ADP-ribose) polymerase inhibitors (PARPi)[5]. While these therapies improve systemic disease control, they may inadvertently increase the likelihood of BM development by allowing time for the seeding and growth of distant metastases. The occurrence of BMs typically indicates an adverse prognostic factor, with a median survival of around 8–12 months after their diagnosis[6].

Treatment options, besides corticosteroids and antiepileptic drugs, include systemic chemotherapy, radiotherapy and surgical resection. However, until now, there is a lack of a common agreement on the therapy[7–8] and the identification of effective biomarkers of brain involvement and prognosis[9–10–11]. Although previous studies have explored the genomic landscape of matched primary tumours and brain metastases[12], limited data exist for EOC-specific populations, particularly at the gene expression level.

This represents a relevant unmet need, especially in the era of personalized medicine, where precise prognostication is essential for empowering clinicians to make well-informed decisions regarding treatment and patient care from the very beginning of the disease[13]

By conducting a multimodal characterisation on a retrospective cohort of primary EOC samples (PT) and their matched BM, we established that BM samples harbour peculiar mutational and gene expression features possibly suitable for targeted therapies, determining that PT samples harbour distinct molecular features that predict the onset of BM.

We identified a distinct brain-metastatic transcriptional profile in EOC with BM, characterized by extracellular matrix remodelling, neuronal–glial phenotypic adaptation, metabolic reprogramming, and heightened proliferative signalling. BM exhibited unique gene expression changes, including upregulation, among others of *AFP* (Alpha-fetoprotein), *GFAP* (Glial Fibrillary Acidic Protein), and *MET* (MET Proto-Oncogene, Receptor Tyrosine Kinase), suggesting neuronal-like adaptation and immune evasion. Gene Set Enrichment Analysis (GSEA) highlighted key pathways such as *MYC* (MYC Proto-Oncogene, BHLH Transcription Factor), *E2F* (E2F Transcription Factor), and *mTORC1* (Mammalian target of rapamycin complex 1) signalling, indicating that EOC cells co-opt brain-specific mechanisms to survive and thrive in the central nervous system (CNS), offering potential biomarkers and therapeutic targets for brain-directed metastasis.

Results

Patients and samples

On a total of 4978 EOC patients treated at Fondazione Policlinico Gemelli IRCCS (FPG) between January 2000 and December 2021, a subset of 111 patients experienced BM (mEOC – 2.2% of total), as previously described *(Figure 1A)*[5]. In this time frame 10 mEOC (mEOC 1-10) patients (0.9% of mEOC) underwent BM surgical resection. For these patients, FFPE tissue samples were collected from both the primary tumour (mEOC_PT) and the corresponding brain metastases (mEOC_BM). The clinical characteristics of the entire population are reported in the *Table*. The median mEOC

patients' age at the diagnosis of EOC was 54 years. Eight patients were affected by high-grade serous ovarian cancer (HGSOC), one by clear cells ovarian cancer (CCOC) and one by endometrioid ovarian cancer (EEOC). *Supplementary Data 1* shows the digitized pathological slides of the PT and the corresponding BM. All patients received first-line chemotherapy with Carboplatin and Paclitaxel, and all of them were platinum-sensitive (relapse after more than 6 months since the last platinum-based chemotherapy). One patient received maintenance treatment with Bevacizumab after the first line of adjuvant chemotherapy. Four patients received platinum-based chemotherapy followed by maintenance therapy at the time of platinum-sensitive relapse (two Bevacizumab and two PARPi). The other patients did not receive maintenance treatments in any setting. The median time frame between the primary EOC diagnosis and the BM was 29.5 months. In six cases, BM were located in the cerebrum, and in four cases, in the cerebellum. In *Supplementary Data 1*, the radiological scans of BM are shown.

BM treatment differed between patients, including surgery, radiotherapy and chemotherapy. Nine out of ten patients died from disease (median overall survival 45 months, min-max: 32-96). The follow-up of the only alive patient is 64 months, and she is currently free of disease *(Figure 1B).* Though numerically small, this paired-sample resource is uniquely poised to unravel the molecular evolution of brain-tropic EOC and to validate our multimodal findings in a clinically impactful setting.

To elucidate the gene expression changes underlying EOC progression to and establishment within the brain, we selected different control populations. First, four healthy brain samples (ctrl_BRAIN) were collected. Median age of the ctrl_BRAIN patients was 55 years, 2 were male and 2 were female; two samples came from hippocampus, one from the cerebral cortex and one from the cerebellum. Second, two healthy ovary samples (ctrl_OVARY) were collected.

We then selected two distinct EOC populations with comparable characteristics to the mEOC cohort. (*Table*) Specifically, primary EOC samples from patients with long-term survival (> 5 years) who did not develop BM (other_EOC_PT). Similar to the mEOC cohort, the mean age of the cohort was 57 years. Eight patients were affected by HGSOC, one by a dedifferentiated EOC. All patients were treated with debulking surgery followed by first-line chemotherapy with Carboplatin and Paclitaxel. Four patients out of nine received maintenance therapy (one with PARPi and the remaining with Bevacizumab. All patients except for one had a platinum-sensitive relapse, median overall survival (OS) was 124 months (min-max: 102-NE).

We next selected non-brain metastatic relapse samples (other_EOC_METS), comprising four lymph node metastases, three bowel metastases, one hepatic metastasis, and one splenic metastasis (*Supplementary Data 2*). All the samples were collected at the time of surgery performed for a platinum-sensitive relapse. All patients have received previous debulking surgery, Carboplatin and Paclitaxel chemotherapy and maintenance treatment with Bevacizumab (except for two patients). Median OS was not reached (95% Confidence Interval, 110-NE). Further clinical characteristics are in the *Table.*

Healthy lymph nodal, hepatic and intestinal tissues (ctrl_HEALTHY1-3) were used as controls.

Samples from other_EOC_PT and ther_EOC_METS populations were not paired. This multi-group design was intended to distinguish transcriptional features unique to brain-tropic EOC from generic metastatic or baseline EOC traits, thus ensuring a clear view of brain-specific adaptations.

DNA Genomic profiling

Somatic sequencing on mEOC_PT and matched mEOC_BM showed very high concordance of single nucleotide variants (SNVs) *(Figure 1C).*

Analysis of SNVs and microsatellite regions allowed to determine that the vast majority of mEOC had a monoclonal origin and maintained a stable tumor mutational burden (TMB) and microsatellite instability (MSI) status *(Figure 1C and Supplementary Data 3A).*

A pathogenic *TP53* variant was identified in 70% of patients, in all cases shared between PT and BM. *PIK3CA* was altered in 20% of patients, specifically patients affected by EEOC and CCOC. Other Tier I and Tier II variants resulted to be either patient's private (*ARID1A* - AT-rich interaction domain 1A) or PM/BM tumor's private (*RET* - Ret Proto-Oncogene, *FAT* - FAT Atypical Cadherin, *TET2* - Tet Methylcytosine Dioxygenase 2). A comprehensive summary of all genes, including full names, deregulation type, GO IDs and related terms, the most representative reference and the assigned functional cluster, is provided in *Supplementary Data 4*.

Copy number variants (CNVs), confirmed 16 chromosomal alterations (6 copy number gains and 10 copy number losses), supported by concordant changes in mRNAs expression (upregulated genes in gains, downregulated in loss) *(Supplementary Data 3B)*. CNV were more frequent in mEOC_BM, potentially reflecting late-arising genomic alterations that promote CNS colonization. Five of ten samples pairs lacked CNV altogether, while mEOC-4 showed losses in *B2M* (Beta-2-Microglobulin) and *MGA* (MAX Dimerization Protein), that were not validated at transcriptional level.

To conclude, although SNVs remained highly conserved between mEOC_PT and mEOC_BM, CNV alterations were more prevalent in the metastatic samples. Clonal evolution analysis further supported a monoclonal origin shared across primary and brain lesions.

RNA Gene expression analysis

We performed a transcriptomic comparison of mEOC_PT and mEOC_BM, along with well-defined control tissues, to elucidate the gene expression changes underlying EOC progression to and establishment within the brain. As RNAseq platform, we employed a 3'-end RNAseq (or 3' Digital Gene Expression – 3'DGE) approach, which is specifically suitable for highly degraded samples, allowing to fully capture the transcriptome profiling by quantifying the terminal portion of any mRNA[14]

We initially employed 3'DGE and performed a cross-comparative analysis of differentially expressed genes (DEGs) across mEOC_BM, mEOC_PT, ctrl_BRAIN, and other_EOC_METS *(Figure 2A).* Additionally, the top five upregulated genes for each comparison (ranked by fold change among significant DEGs) are displayed in the adjacent panels. The full list of DEGs, including Symbol, p-adj, log2FoldChange is displayed in *Supplementary Data 5*. To establish a reference profile of tumour-specific alterations, we first compared mEOC_BM against ctrl_BRAIN. This analysis identified 2,845 upregulated and 1,664 downregulated genes in mEOC_BM (*Figure 2A, right*). While many of these changes reflect lineage-specific expression, the top five upregulated genes - *RAB25* (RAB25, Member RAS Oncogene Family), *PI3* (Peptidase Inhibitor 3), *MISP* (Mitotic Spindle Positioning), *TMPRSS4* (Transmembrane Serine Protease 4), and *UGT2B7* (UDP Glucuronosyltransferase Family 2 Member B7) - suggest CNS-specific adaptations. Their selective elevation in BM suggests that EOC cells exploit these pathways to cope with the restrictive CNS microenvironment.

Next, to distinguish brain-specific drivers beyond generic metastatic traits, we compared mEOC_BM to other_EOC_MET *(Figure 2A, left).* Among the 164 significantly upregulated genes, *AFP* exhibited the highest induction, followed by *GFAP*, *ELAVL3* (ELAV Like RNA Binding Protein 3), and *HCN2* (Hyperpolarization Activated Cyclic Nucleotide Gated Potassium and Sodium Channel 2). Although *GFAP*, *ELAVL3*, and *HCN2* could partially stem from surrounding neuronal or glial cells, their recurrent presence with high expression levels suggests that EOC cells may acquire or mimic neuroglial traits to foster survival in the CNS. Meanwhile, *AFP*, which we later observe in primary

EOC as well, may exert immunoregulatory or neurotrophic influences, strengthening the concept of an early CNS-compatible phenotype.

By comparing mEOC_BM with matched mEOC_PT, we discovered 33 upregulated and 115 downregulated genes *(Figure 2A, bottom).* Late-stage transcriptomic shifts during CNS colonization were evident, with *GFAP* emerging as the most differentially expressed gene. Integrating these data, we defined a core brain-metastatic gene signature - *SQLE* (Squalene Epoxidase), *ATAD5* (ATPase Family AAA Domain Containing 5), *LAMC3* (Laminin Subunit Gamma 3), *ADSL* (Adenylosuccinate Lyase), and *LINC00562* (Long Intergenic Non-Protein Coding RNA 562) - consistently overexpressed in mEOC_BM (all padj < 0.05) *(Figure 2B).* Notably, *LAMC3*, involved in cortical lamination, may facilitate CNS-specific ECM remodelling and metastatic engraftment[15].

To investigate how these molecular changes converge at a pathway level, we performed GSEA on each comparison: mEOC_BM vs. ctrl_BRAIN; mEOC_BM vs. other_EOC_METS; and mEOC_BM vs. mEOC_PT *(Figure 2C).*

In the comparison of mEOC_BM with healthy brain tissue, *E2F* targets, G2M checkpoint, Interferon gamma response and Estrogen response late. Moreover, we noted an enrichment in the *MYC* targets, signalling a transition toward hyperproliferation and heightened transcriptional output. Concomitant upregulation of stress-related/inflammatory programs (TNFα signalling) suggests an immune-evading or pro-inflammatory shift suitable for metastatic colonization.

By contrasting mEOC_BM with other_EOC_METS, marked emphasis on SPERMATOGENESIS, *mTORC1*_SIGNALING, *E2F* targets, and G2M checkpoint emerged. Finally, comparing mEOC_BM with mEOC_PT confirmed a trend toward persistent activation of *MYC*, *E2F* pathways, G2M checkpoint, and SPERMATOGENESIS in metastases, highlighting the final transcriptional refinements EOC cells acquire upon CNS invasion. Altogether, these transcriptomic data reveal a brain-tropic phenotype underpinned by ECM remodelling, tumor-glial interaction, metabolic reconfiguration, and heightened proliferative signals.

To determine whether mEOC_PT harbour transcriptional clues indicating future brain metastatic competence, we employed 3'DGE and assessed DEGs relative to both ctrl_OVARY and other_EOC_PT *(Figure 3A).* For each comparison, the adjacent panels show the top five upregulated genes (selected by the highest fold change among significant DEGs) to summarize the strongest early transcriptional drivers.

Comparisons of mEOC_PT with ctrl_OVARY revealed upregulation of *FXYD3* (FXYD Domain Containing Ion Transport Regulator 3), *ESRP1* (Epithelial Splicing Regulatory Protein 1), *RAB25*, *BICDL2* (BICD Family Like Cargo Adaptor 2), and *CKMT1B* (Creatine Kinase, Mitochondrial 1B) *(Figure 3A, left).*

In contrast, comparisons of mEOC_PT with other_EOC_PT identified *S100P* (S100 Calcium Binding Protein P), *NCCRP1* (*NCCRP1*, F-Box Associated Domain Containing), *PIGR* (Polymeric Immunoglobulin Receptor), *AFP*, and *DNER* (Delta/Notch Like EGF Repeat Containing) as the most highly upregulated *(Figure 3A, right).*

The intersection of these comparisons uncovered 13 genes uniquely upregulated in mEOC_PT - *AFP*, *S100P*, *GDF15* (Growth Differentiation Factor 15), *NCCRP1*, *AP1B1* (Adaptor Related Protein Complex 1 Subunit Beta 1), *NUDT14* (Nudix Hydrolase 14), *NDUFA4L2* (NDUFA4 Mitochondrial Complex Associated Like 2), *FGFR3* (Fibroblast Growth Factor Receptor 3), *TFCP2L1* (Transcription Factor CP2 Like 1), *TSPAN1* (Tetraspanin 1), *SLC29A4* (Solute Carrier Family 29 Member 4), *TXNL4A* (Thioredoxin Like 4A), and *SERINC2* (Serine Incorporator 2) - collectively suggesting a "premetastatic" program favouring CNS colonization *(Figure 3B).* To contextualize these individual gene findings, we conducted GSEA on mEOC_PT relative to ctrl_OVARY and other_EOC_PT *(Figure 3C).* In the mEOC_PT vs. ctrl_OVARY comparison, pathways associated with Neuroactive ligand-receptor interaction and ECM interaction were prominently enriched, hinting that certain EOC primaries are already primed for microenvironmental cues critical to metastasis. Among these, the Neuroactive ligand–receptor interaction gene set notably emerged, suggesting that EOC cells may engage in neuronal-like signalling or receptor-mediated communication — potentially reflecting early adaptive traits that later contribute to tumor–neural interactions observed in advanced brain metastases.

In the mEOC_PT vs. other_EOC_PT comparison, Neuroactive ligand-receptor interaction reappeared, affirming that a subset of primary tumours expresses an ECM-focused, immune-evasive, or neuroactive phenotype absent in non-brain-metastatic EOC. This synergy of ECM remodelling, stress/immune pathways, and neuronal-like interactions may represent a cohesive "premetastatic signature," enabling EOC cells to more readily seed distant organs such as the brain.

Building upon our observation of neuroactive ligand–receptor enrichment in mEOC_PT, we next sought to identify membrane-bound or secreted factors potentially relevant for EOC cells' adaptation to the CNS. Pairwise comparisons of upregulated genes from mEOC_PT vs. other_EOC_PT and

mEOC_BM vs. other_EOC_METS identified 15 transcripts consistently elevated in both the primary site and brain lesions *(Figure 4A).* Such overlap suggests a recurrent signaling axis that arises early and persists into overt brain colonization.

To further characterize these trasnscripts, we applied an agnostic filtering strategy: genes were retained if annoted with GO terms for plasma membrane [GO:0005886] or extracellular space [GO:0005615]) and subsequently classified as ligands or receptors using the OmniPathR (v3.14.0) database. Next, we further cross-referenced these candidates with CNS-related GO terms as Nervous system development [GO:0007399] and Synaptic transmission [GO:0007268]. Through this multi-step filtering, we identified three candidate ligand/receptor genes consistently upregulated across tumor stages: *MET*, *GDF15*, and *S100A9.* Notably, GDF15 was already highlighted among intersected genes in the premetastatic signature (*Figure 3B*). The network representation (*Figure 4B*) depicts *MET*, linked here to ECM-modulatory genes such as *LRG1* (Leucine Rich Alpha-2-Glycoprotein 1), *TIMP3* (TIMP Metallopeptidase Inhibitor 3), *DCN* (Decorin), and *ADAM17* (ADAM Metallopeptidase Domain 17), emphasizes the receptor's known roles in cell motility and invasion, aligning with earlier GSEA findings implicating ECM receptor interactions in EOC primaries. *GDF15*, in association with its receptor *GFRAL* (GDNF Family Receptor Alpha Like), a pairing implicated in stress response and a metabolic reprogramming axis relevant for hypoxic and nutrient-limited CNS niche. We next examined the expression levels of *MET, GDF15* and *S100A9* across mEOC_PT, mEOC_BM, other_EOC_PT, and other_EOC_METS *(Figure 4C).* All genes were significantly upregulated in mEOC_PT and mEOC_BM compared to their respective control groups (DESeq2 padj < 0.05).

Altogether, these results nominate *MET*, *GDF15*, and *S100A9* as candidate ligand–receptor nodes that underlie EOC progression into the CNS. Their upregulation from primary tumors to brain-metastatic lesions highlights both biomarker potential for predicting CNS risk and novel therapeutic avenues to intercept metastatic dissemination.

Discussion

Here, we provided a multimodal analysis of BM derived from EOC, through a comprehensive genome profiling and a gene expression analysis of matched PT and BM samples. Although BM remain relatively infrequent, their emergence is clinically relevant, reinforcing the need for early predictive markers and actionable targets.

For patients with isolated BM relapse, surgery remains a viable therapeutic option. However, approximately 50% of these patients are deemed ineligible due to concomitant extracranial disease, anatomical inaccessibility, or poor overall clinical status[16]. Consequently, the acquisition of matched primary and metastatic tissue is technically and logistically challenging. In this context, our paired-sample cohort—though limited in size—represents a valuable and rare resource for dissecting the molecular evolution of brain-tropic EOC. To the best of our knowledge, this is the largest and only cohort of multimodal analysis performed on matched PT and BM in EOC patients. Previous studies have identified possible genomic signatures of multi-organ diffusion[17]. Nevertheless, that study was limited to DNA-only analysis, whereas we identified major patterns primarily at the RNA level.

Our findings demonstrate that EOC PT and matched BM exhibit many similarities in terms of genomic variants and gene expression. Nonetheless, certain pathways associated with cell cycle progression, *MYC* targets, cellular growth, and ECM interaction shed light on the mechanisms underlying brain colonization and metastatic fitness in the neuronal microenvironment.

It has been previously shown that EOC BRCA mutated patients have a higher incidence of BM (3% vs 0.6% of BRCA-wild type patients)[17]-[18]. However, in our cohort, no patient showed a BRCA mutation, nor other somatic variants that may suggest a germline[19] origin. This, together with the almost superimposable genomic profile, indicates that biological mechanisms of adaptation to CNS, rather than germline mutations, could be related to the BM in the EOC population.

Our results identify potential biomarkers of BM onset. In particular, *AFP* emerged as upregulated both in primary EOC that metastasized to the brain and in brain healthy tissues. *AFP* is a protein predominantly expressed during fetal development, with serum levels significantly decreasing after birth as *AFP* gene expression is downregulated. In adults, *AFP* is widely recognized as a biomarker for ovarian germ cell tumors. Interestingly, elevated *AFP* levels have also been reported in at least four distinct neurodegenerative disorders. These disorders, inherited as autosomal recessive traits, are characterized by a combination of cerebellar ataxia, abnormal ocular movements, and peripheral neuropathy. This may represent a potential link between *AFP* expression and nervous system[20], still unexplored in cancer. The consistent overexpression of *AFP* and additional candidates such as *TFCP2L1* and *ESRP1* provide a foundation for developing predictive biomarkers and highlight early molecular divergence that may inform risk stratification and therapeutic intervention in EOC.

GFAP emerged as upregulated in mEOC_BM. This is a component of the glial cytoskeleton and a candidate biomarker of glial cell damage. Moreover, consistent with our data, it has been previously described as a serum biomarker of BM in patients with metastatic breast cancer[21].

In BM, the hallmarks of the *MYC* target were altered. High expression of hallmarks of *MYC* targets have already been correlated with higher cell proliferation, higher stage, pathological grade, and worse subtype in a large population of breast cancer[22]. Moreover, *MYC* family genes are found overexpressed in more than half of all brain cancers, highlighting its role as one of the most important oncogenes. *MYC* proteins are involved in brain tumor initiation, maintenance and progression[23]. LAMC3, which is crucial for cortical lamination—as shown by laminar disorganization in LAMC3 deficient mice—may also play a role in CNS-specific extracellular matrix remodelling and metastatic engraftment, given the broader function of laminin γ-chains in facilitating cell adhesion, migration, and metastasis[24]. Moreover, it has been previously described in EOC progression[22]. Crucially, in our data, the intersection of *LAMC3* and *MYC* target genes within the *MET* signalling network, a pathway recognized for bolstering cell motility, introduces a compelling avenue for future research.

The network analysis prioritized *MET*, *GDF15*, and *S100A9* as elevated both in mEOC_PT and mEOC_BM. *S100A9* is a protein expressed in myeloid-derived cells involved in controlling immunological homeostasis and cell metabolism. It is considered a tumor promoter, by influencing tumor genesis, progression, and metastasis[23]. It has been reported that high *S100A9* expression was associated with BM and shorter PFS in EGFR-mutated lung cancer patients treated with Osimertinib. Moreover, targeting the *S100A9–ALDH1A1–RA* signalling axis reduced BM in mice models [25].

Some strengths and limitations must be acknowledged. We enlightened some of the mechanisms that could explain BM onset and potential druggable targets. Nevertheless, some important caveats need to be acknowledged. First, the sample size in all comparisons was limited, and differential expression analyses did not account for potential confounders such as treatment history or tissue type. Second, no independent validation was performed, and brain regions were not matched between cases and controls, introducing substantial intertumor heterogeneity. Moreover, the patients included in the study received treatment over an extended period, when targeted therapies such as Bevacizumab or PARPi were not routinely administered. Notably, PARPi pharmacokinetics demonstrated a possible brain penetration in mice, but with differences between molecules. Substantial functional and genomic alterations in the tumour have been recorded following exposure to these drugs, potentially leading to profound changes in its molecular profile[22-28-29]. This may limit the applicability of our findings. Finally, spatial and temporal heterogeneity were not considered, but they should be acknowledged in future studies to gain a more comprehensive understanding.

In conclusion, this study provides novel insights into the molecular underpinnings of EOC BM, emphasizing the need for further research to validate these findings and explore their translational potential in improving clinical outcomes.

Methods

The present study was conducted following the guidelines of the Declaration of Helsinki (1984) and subsequent revisions. The methods were performed in accordance with relevant guidelines and regulations. with the approval of the Ethical Committee of Fondazione Policlinico Universitario Agostino Gemelli IRCCS (protocol ID: METACER-OV, date of approval: 07/04/2022, ID number: 4865). We retrospectively collected clinical data from EOC patients treated at Fondazione Policlinico Gemelli IRCCS between January 2000 and December 2021. Inclusion criteria were as follows: diagnosis of BM confirmed by computed tomography scan, magnetic resonance imaging, and/or positron emission tomography conducted during follow-up, for monitoring treatment response, or in response to symptoms, with no prior brain-directed therapy. Exclusion criteria included a history of other malignancies or CNS diseases unrelated to brain metastases. Written informed consent for the publication of clinical and molecular data, including photos. was obtained from all patients or their legal representatives before they participated in the study. As a control for RNA-seq analysis, we selected comparable EOC populations who did not experience BM. Specifically, we collected the primary EOC formalin-fixed, paraffin-embedded (FFPE) samples of 9 long-term survivor patients (>5 years) who did not experience BM (other_EOC_PT); and the FFPE of relapse samples from 9 long-term survivor patients (>5 years) patients who experienced relapses at different sites than the brain (other_EOC_METS), specifically four were lymph node metastases, three were bowel metastases, one was a hepatic metastasis, and one a splenic metastasis. Moreover, healthy tissues of the brain obtained by autoptic samples (ctrl_BRAIN 1-4), ovary (ctrl_OVARY 1-2) and tissue corresponding to metastasis other than brain - lymph nodes, liver and bowel - (ctrl_HEALTHY1-3) were collected. *Figure 1A* shows the study design.

A comprehensive genomic profiling (CGP) assay was performed using Illumina TruSight Oncology 500 high throughput assay. After a careful evaluation by a dedicated pathologist, only samples showing ≥20% of tumor cellularity were processed. Nucleic acids were extracted using the AllPrep DNA/RNA FFPE Kit (Qiagen, Hilden, Germany). The quantity and quality of extracted DNA and RNA were evaluated using Qubit and Agilent TapeStation, respectively. Libraries were prepared with specific panels (TruSight Oncology 500 High-Throughput Assay, Illumina) and sequencing was performed with the Illumina Novaseq6000 platform using the 2x101 bp paired-end sequencing

protocol. Raw sequencing data underwent quality control and bioinformatic analysis using Illumina Software TSO500 Dragen solid v2.5 and a pipeline within the Clinical Genomics Workspace software platform from Velsera. An evaluation of SNVs, insertions/deletions (indels) and CNVs in 523 genes, as well as known and unknown fusions and splicing variants in 55 genes was provided. It also estimates TMB and MSI.

SNVs and indels underwent a multistep filtering process characterized by the application of four primary criteria.

Variant annotation was performed using Ensembl Variant Effect Predictor (VEP)[30], accession date: 1st of October 2024. Oncogenicity annotations originated from the OncoKB database and specifically referred to genetic mutations that drive the development of cancers or influence their response to treatments[31].

Initially, variants with an allelic frequency exceeding 1%, as reported by the Genome Aggregation Database (GnomAD)[32], were excluded.

Subsequently variants with VAF under 2% were excluded.

In addition, variants with a detrimental impact on the protein, including frameshift, splice donor, stop gained, splice acceptor, start lost, in-frame insertion, and in-frame deletion, were preserved.

The assessment of CNVs was conducted considering any level of variations in the number of copies, considering amplifications defined as ≥ 5 copies and homozygous deletions. The analysis does not include the detection of CNVs involving single exons or complete gene deletions.

To enhance the rigor of our CNVs calls, we employed transcriptomic data for validation. Specifically, for each cohort —mEOC_PT and mEOC_BM—RNA expression levels were used as an independent confirmation. Within each group, a gene was considered amplified if its transcript abundance exceeded the 75th percentile of that group's expression distribution, and conversely, a deletion was confirmed if the expression was below the 25th percentile.

To model tumor evolution, we employed Pyclone VI[33]. This algorithm facilitates the inference of clonal architecture and the tracking of spatial and temporal patterns in tumor evolution. The results were subsequently visualized using R V. 4.3.2 packages including ggplot2, fishplot and clonevol. ClonEvol is a tool for the reconstruction and interpretation of clonal evolution[34]. It uses the clustering of heterozygous variants identified using other tools as input to infer consensus clonal evolution trees and estimate the cancer cell fraction (also called clonal frequency) of the clones in individual samples.

Total RNA was micro-dissected and purified from paraffin-embedded tumor tissue with Maxwell® RSC RNA FFPE Kit (Promega), following manufacturer' instructions and quantified using the Qubit

2.0 Fluorometer (Thermo Fisher Scientific). Libraries were prepared from 250 ng of total RNA using the 3′ Digital Gene Expression (3′DGE) mRNA-seq pipeline (NEGEDIA s.r.l.), which includes rigorous quality-control steps to minimize technical variability. Libraries were sequenced on an Illumina NovaSeq 6000 platform using a 100-cycle, single-end run configuration. Raw sequencing reads were quality-filtered using the BBtools software suite (specifically the bbduk utility) to remove low-quality bases and adapter contaminants. Cleaned reads were aligned to the human reference genome GRCh38 using the STAR aligner (v2.6). Gene-level counts were obtained using HTSeq-count using GENCODE annotations for GRCh38. The resulting raw counts were further filtered to remove lowly expressed genes (threshold: at least one count per million in at least two samples). Normalized expression levels were obtained via counts per million (CPM), and log2 transformations were applied where indicated. We employed a negative binomial model (DESeq2 v.1.46.0) with Benjamini–Hochberg p-adj correction for differential expression analysis.

To identify DEGs, we performed multiple pairwise comparisons as indicated in the text. Significant DEGs were defined as those with an absolute log2 fold-change ($|\log2FC| \geq 1$ and adjusted p-value (padj) < 0.05. Venn diagrams were used to illustrate overlapping DEGs across specific comparisons. Additionally, the top five upregulated genes (ranked by fold-change among significant DEGs) are shown in the adjacent panels for each comparison. Gene annotation was performed using org.Hs.eg.db (v 3.20.0) and GO.db (v 3.20.0) via the AnnotationDbi interface in R (V 1.68.0). We mapped Ensembl IDs (from DEGs) to gene symbols and GO terms (BP, MF, CC). Subsequently, we refined annotations using a literature-based curation for each gene to tailor functions relevant to ovarian cancer metastasis. For all boxplot visualizations, statistical significance was assessed using Student's t-test comparing mEOC_BM or mEOC_PT to the respective groups, with thresholds indicated as $p < 0.05$ (*) and $p < 0.01$ (**).

GSEA was performed to identify hallmark pathways enriched in each comparison. Genes were ranked based solely on the $\log_2$ fold change obtained from differential expression analysis. The pre-ranked gene list was generated by ordering genes in descending order of $\log_2$ fold change. Normalized enrichment scores (NES) and false discovery rate (FDR) values were calculated using the default settings of the GSEA software (Broad Institute). Significant pathways were defined as those with $|NES| \geq 1.5$ and $FDR \leq 0.05$. Pathway analyses were carried out using the R package *clusterProfiler* (v4.14.4) in conjunction with the *org.Hs.eg.db* annotation database (v3.20.0). Hallmark gene sets were retrieved via the *msigdbr* package (v7.5.1). Additionally, KEGG pathway analysis was performed only for the mEOC_PT vs ctrl_OVARY and mEOC_PT vs other_EOC_PT comparisons to provide further insights into functional enrichments.

To systemically identify potential ligand–receptor genes potentially involved in EOC adaptation to the CNS, we adopted an agnostic filtering approach. We first screened differentially upregulated genes from mEOC_PT and mEOC_BM relative to their respective controls (other_EOC_PT and other_EOC_MET). From this set, we retained only transcripts annotated for membrane-associated or secreted proteins, with GO terms that specify membrane or extracellular localization (plasma membrane [GO:0005886], extracellular space [GO:0005615]). We then employed the OmniPathR (v.3.14.0) database to classify these filtered genes as ligands or receptors, focusing on those with known or putative with known signalling functions. To ensure potential relevance to CNS, we further intersected these candidates with GO terms associated with nervous system development [GO:0007399], synaptic transmission [GO:0007268]. Network visualization was conducted in Cytoscape (v.3.10.3), with nodes representing ligands/receptors and edges denoting curated interaction.

Acknowledgements

We are thankful for the support of NEGEDIA srl.

DC is funded by Fondazione Telethon Core Grant, Armenise-Harvard Foundation Career Development Award. DC and MC are funded by Italian Ministry of Health (Piano Operativo Salute Traiettoria 3, T3-AN-09, “Genomed”; Ricerca Finalizzata 2021, “genOMICA”; MCNT2 2023, “EUCARDIS”), Italian Ministry of University and Research and European Union (Next Generation EU - MUR-PRIN-2022 CUP 2022T7XP29 and 2022HM5LFW, Project PNC 0000001 D3-4-Health). LV was supported by a AIRC Fellowship for Italy.

Competing interests

Davide Cacchiarelli is founder, shareholder, and consultant of NEGEDIA S.r.l.

Giovanni Scambia is consultant for AstraZeneca, MSD and Covidien AG, a Medtronic company. Giovanni Scambia is member of the speakers bureau/honoraria for Olympus Europa SE & CO. KG, Baxter Healthcare SA, Intuitive Surgical Inc., GlaxoSmithKline S.p.A. Giovanni Scambia is member of the advisory board/advisory committee of TESARO Bio Italy S.r.l. Johnson & Johnson.

Anna Fagotti has received grants/research support from AstraZeneca and MSD. Anna Fagotti is member of the advisory board of GlaxoSmithKline. Anna Fagotti is member of the speakers/honorary board of Covidien (Medtronic), GSK, pharmaand GmbH and AbbVie. Anna Fagotti is consultant for Oncoinvent AS.

Claudia Marchetti is consultant/advisory board member for Clovis, Pharmamar, GSK, AstraZeneca, AbbVie, pharmaand GmbH and MSD. Claudia Marchetti has received travel accommodation from Pharmamar and Roche.

Camilla Nero is member of the speakers bureau/honoraria for AstraZeneca, GSK, MSD, GH and Illumina. Camilla Nero is member of the advisory board/advisory committee of AstraZeneca and MSD. Camilla Nero has received grants/research support from AstraZeneca and GH. Camilla Nero has received travel accommodation from AstraZeneca, MSD and Illumina.

Data availability

Due to European General Data Protection Regulation (GDPR) and institutional data protection policies, we are unable to publicly release the raw sequencing data (FASTQ files) because they contain potentially identifiable genomic information. However, to ensure transparency and reproducibility, we have made processed RNA-seq count matrices (CPM-normalized values). For researchers requiring access to the raw sequencing files, such data can be provided upon reasonable request, and the transfer will require the completion of a data transfer agreement with our institution in compliance with GDPR.

Figure legends

Figure 1: Cohort Selection, Survival Trajectories, and Genomic Landscape in Brain-Metastatic EOC

(A) Consort Diagram of the study population **(B)** Swimmer plot. Each horizontal bar represents one patient. HGSOC, High-grade serous ovarian cancer; CCOC, Clear cells ovarian cancer; EEOC, Endometrioid epithelial ovarian cancer; WT, wild type.

(C) Oncoplot illustrates the mutational profiles of patients from mEOC1 to mEOC10, with both primary (P) and metastatic (M) tumor samples represented for each patient. The top annotation provides clinical information, including age at diagnosis, tumor stage and tumor clonality. Tumor Mutational Burden (TMB) and Microsatellite Instability (MSI) are depicted as bar plots for both primary and metastatic tumors. The color-coded legend below classifies TMB as High, Medium or Low and MSI as Stable. Genomic alterations are categorized into single-nucleotide variants (SNVs) and small insertions/deletions (InDels), Copy Number Variations (CNVs) and Gene Fusions. SNV/InDel mutations are further annotated based on clinical relevance, with asterisks indicating Tier I and Tier II classifications, while color coding differentiates mutation types. CNVs are stratified into gain/loss and gain/loss supported categories, represented by distinct colors.

*created with Biorender

Figure 2: A specific transcriptional signature defines the EOC brain metastasis

(A) Venn diagram illustrating intersected differentially expressed genes (DEGs) uniquely upregulated (red) and downregulated (blue) in epithelial ovarian cancer brain metastases (mEOC_BM) compared with primary ovarian tumors (mEOC_PT), non-CNS metastatic sites (other_EOC_MET), and healthy brain tissue (ctrl_BRAIN). Highlighted are top 5 genes specifically upregulated in each pairwise comparison.

(B) Boxplots depicting normalized gene expression (log2 CPM counts) across the entire cohort (mEOC_BM, mEOC_PT, ctrl_BRAIN, ctrl_OVARY, otherEOC_PT, other_EOC_MET, ctrl_HEALTHY) for selected candidate genes consistently enriched in brain metastases: *SQLE*, *ADSL*, *LAMC3*, *ATAD5*, and *LINC00562*. Statistical comparisons were performed using Student's t-test against mEOC_BM, with significance thresholds annotated (* $p < 0.05$; ** $p < 0.01$)

(C) Dot plots showing Gene Set Enrichment Analysis (GSEA) results for hallmark pathways significantly enriched in mEOC_BM relative to ctrl_BRAIN (left), other_EOC_MET (right, top), and matched mEOC_PT (right, bottom). Pathways are ranked by normalized enrichment score (NES). Dot size reflects the number of contributing genes; dot color indicates statistical significance (adjusted p-value).

Figure 3: Early transcriptional signature predicts ovarian cancer predisposition to brain metastasis

(A) Venn diagrams representing the intersection of significantly upregulated (red) and downregulated (blue) genes in primary epithelial ovarian cancer samples predisposed to brain metastasis (mEOC_PT) when compared to healthy ovarian tissue (ctrl_OVARY) and primary ovarian tumors without brain metastatic potential (otherEOC_PT). Highlighted are the top five genes uniquely elevated in each comparison. Statistical comparisons were performed using Student's t-test against mEOC_PT, with significance thresholds annotated (* $p < 0.05$; ** $p < 0.01$).

(B) Boxplots illustrating normalized gene expression (log2 CPM counts) for the 13 intersected genes (*AP1B1*, *SERINC2*, *TXNL4A*, *SLC29A4*, *AFP*, *NUDT14*, *NDUFA4L2*, *FGFR3*, *TFCP2L1*, *TSPAN1*, *GDF15*, *S100P*, *NCCRP1*) across mEOC_BM, mEOC_PT, ctrl_BRAIN, ctrl_OVARY, other_EOC_PT, other_EOC_METS.

(C) Dot plots showing Gene Set Enrichment Analysis (GSEA), displaying significant KEGG pathways enriched in mEOC_PT compared with ctrl_OVARY (left) and otherEOC_PT (right). Dot size represents the number of enriched genes, while color intensity indicates statistical significance (adjusted p-value).

Figure 4

Ligand–receptor interactions predict ovarian cancer adaptation to the brain microenvironment

(A) Venn diagram depicting upregulated DEGs in mEOC_PT vs. other_EOC_PT and mEOC_BM vs. other_EOC_METS

(B) Ligand–receptor network of overlapping upregulated genes, highlighting nodes (ligands in green, receptors in blue, dual-function genes in red): MET, *GDF15*, and *S100A9* as key hubs.

(C) Boxplots of *MET* and *S100A9* (log2 CPM counts) illustrating higher expression in mEOC_PT and mEOC_BM relative to other groups.

Supplementary Data 1: Digitalized histopathological slides and radiological scans of mEOC samples.

Representative hematoxylin and eosin (H&E) images of mEOC_PT and matched mEOC_BM from the study cohort (n = 10), Where available, radiological scans (MRI or CT) illustrate the anatomical BM sites.

Supplementary Data 2: Digitalized histopathological slides of other_EOC_PT and other_EOC_MET

Representative hematoxylin and eosin (H&E)–stained sections of other_EOC_PT (n = 9). and other_EOC_MET (n = 9). The anatomical site of each metastatic lesion is indicated.

Supplementary Data 3: Clonality and CNV–expression analysis in mEOC

(A) PyClone analysis showing clonal architecture of matched primary tumors (mEOC_PT) and brain metastases (mEOC_BM), with clusters defined by mean variant allele frequency (VAF).

(B) Gene expression (log2 CPM) for selected genes (*ARID1B*, *CCNE1*, *CDK6*, *EZH2*, *KRAS*, *MCL1*, *MET*, *MYCL1*, *MYC*, *RB1*) analyzed to confirm CNV events. Boxplots show first–third quartile ranges for primaries (green) and metastases (orange), with single-sample annotations for amplification (green dots) or deletion (blue dots).

Supplementary Data 4: Summary of genes

The table provides a comprehensive summary of all genes, including full names, type of deregulation, GO IDs and related terms, most representative reference, and assigned functional cluster.

Supplementary Data 5: List of DEGs

The table provides the full list of DEGs, including Symbol, p-adj and log2FoldChange.

583

584

585 **Table**

Table: Clinical, pathological, and survival characteristics of patients included in the study and matched controls without BM

	Cases	Controls	
Characteristics	mEOC n=10	other_EOC_PT n=9	other _EOC_METS n=9
Mean age, years	53.7	57	47.4
Histotype			
EEOC	1	0	1
HGSOC	8	8	8
CCOC	1	0	0
Dedifferentiated	0	1	0
BRCA status			
Wild type	9	4	5
BRCA1 mutated	0	3	3
BRCA2 mutated	1	2	1
2016 FIGO stage			
IA	1	0	0
IIIA2	2	0	0
IIIB	0	1	1
IIIC	8	7	8
IVB	0	1	0
Status at follow-up			
DOD	9	4	2
AWD	0	3	4
NED	1	2	3

EEOC: Endometrioid ovarian cancer; HGSOC: High grade serous ovarian cancer; CCOC: clear cells ovarian cancer; DOD: Dead of disease; AWD: alive with disease; NED: Not evidence of disease

586

587 **References**

588 [1] Amate P, Huchon C, Dessapt AL, Bensaid C, Medioni J, Le Frère Belda MA, Bats AS, Lécuru FR. Ovarian
589 cancer: sites of recurrence. Int J Gynecol Cancer. 2013 Nov;23(9):1590-6. doi:
590 10.1097/IGC.0000000000000007. PMID: 24172095.
591 [2] Piura E, Piura B. Brain metastases from ovarian carcinoma. ISRN Oncol. 2011;2011:527453. doi:
592 10.5402/2011/527453. Epub 2011 Dec 1. PMID: 22191058; PMCID: PMC3236423.
593 [3] Pakneshan S, Safarpour D, Tavassoli F, Jabbari B. Brain metastasis from ovarian cancer: a systematic review.
594 J Neurooncol. 2014 Aug;119(1):1-6. doi: 10.1007/s11060-014-1447-9. Epub 2014 May 1. PMID: 24789253.

[4] Alizzi Z, Roxburgh P, Cartwright D, McLaren A, Park S, Jones R, Greening S, Hudson E, Green C, Gray S, Khalique S, Karteris E, Hall M. Description of a Retrospective Cohort of Epithelial Ovarian Cancer Patients with Brain Metastases: Evaluation of the Role of PARP Inhibitors in this Setting. J Clin Med. 2023 Mar 25;12(7):2497. doi: 10.3390/jcm12072497. PMID: 37048581; PMCID: PMC10095324.

[5] Sassu CM, Marchetti C, Russo G, Minucci A, Boccia SM, Benato A, Nero C, Piermattei A, Mattogno PP, Giannarelli D, Ferrandina G, Olivi A, Fagotti A, Scambia G. Epithelial ovarian cancer and brain metastases: might the BRCA status, PARP inhibitor administration, and surgical treatment impact the survival? Int J Gynecol Cancer. 2024 Jan 5;34(1):88-98. doi: 10.1136/ijgc-2023-004980. PMID: 38805344.

[6] Bahat Z, Cakmak VA, Cakir E. Brain metastasis from ovarian carcinoma: Analysis of eight cases from a single radiotherapy center. Taiwan J Obstet Gynecol. 2020 Sep;59(5):711-717. doi: 10.1016/j.tjog.2020.07.015. PMID: 32917323.

[7] Marchetti C, Ferrandina G, Cormio G, Gambino A, Cecere S, Lorusso D, De Giorgi U, Bogliolo S, Fagotti A, Mammoliti S, Narducci F, Bergamini A, Scollo P, Biglia N, Breda E, Tamberi S, Marinaccio M, Angioli R, Salerno L, Eusebi MC, Loizzi V, Scambia G, Panici PB. Brain metastases in patients with EOC: Clinico-pathological and prognostic factors. A multicentric retrospective analysis from the MITO group (MITO 19). Gynecol Oncol. 2016 Dec;143(3):532-538. doi: 10.1016/j.ygyno.2016.09.025. Epub 2016 Oct 5. PMID: 27717490.

[8] Cohen ZR, Suki D, Weinberg JS, Marmor E, Lang FF, Gershenson DM, Sawaya R. Brain metastases in patients with ovarian carcinoma: prognostic factors and outcome. J Neurooncol. 2004 Feb;66(3):313-25. doi: 10.1023/b:neon.0000014516.04943.38. PMID: 15015663.

[9] Pectasides D, Aravantinos G, Fountzilas G, Kalofonos C, Efstathiou E, Karina M, Pavlidis N, Farmakis D, Economopoulos T, Dimopoulos MA. Brain metastases from epithelial ovarian cancer. The Hellenic Cooperative Oncology Group (HeCOG) experience and review of the literature. Anticancer Res. 2005 Sep-Oct;25(5):3553-8. PMID: 16101179.

[10] Dagogo-Jack I, Shaw AT. Tumour heterogeneity and resistance to cancer therapies. Nat Rev Clin Oncol. 2018 Feb;15(2):81-94. doi: 10.1038/nrclinonc.2017.166. Epub 2017 Nov 8. PMID: 29115304.

[11] Bashashati A, Ha G, Tone A, Ding J, Prentice LM, Roth A, Rosner J, Shumansky K, Kalloger S, Senz J, Yang W, McConechy M, Melnyk N, Anglesio M, Luk MT, Tse K, Zeng T, Moore R, Zhao Y, Marra MA, Gilks B, Yip S, Huntsman DG, McAlpine JN, Shah SP. Distinct evolutionary trajectories of primary high-grade serous ovarian cancers revealed through spatial mutational profiling. J Pathol. 2013 Sep;231(1):21-34. doi: 10.1002/path.4230. PMID: 23780408; PMCID: PMC3864404.

[12] Brastianos PK, Carter SL, Santagata S, Cahill DP, Taylor-Weiner A, Jones RT, Van Allen EM, Lawrence MS, Horowitz PM, Cibulskis K, Ligon KL, Tabernero J, Seoane J, Martinez-Saez E, Curry WT, Dunn IF, Paek SH, Park SH, McKenna A, Chevalier A, Rosenberg M, Barker FG 2nd, Gill CM, Van Hummelen P, Thorner AR, Johnson BE, Hoang MP, Choueiri TK, Signoretti S, Sougnez C, Rabin MS, Lin NU, Winer EP, Stemmer-Rachamimov A, Meyerson M, Garraway L, Gabriel S, Lander ES, Beroukhim R, Batchelor TT, Baselga J, Louis DN, Getz G, Hahn WC. Genomic Characterization of Brain Metastases Reveals Branched Evolution

and Potential Therapeutic Targets. Cancer Discov. 2015 Nov;5(11):1164-1177. doi: 10.1158/2159-8290.CD-15-0369. Epub 2015 Sep 26. PMID: 26410082; PMCID: PMC4916970.

[13] Hao Q, Li J, Zhang Q, Xu F, Xie B, Lu H, Wu X, Zhou X. Single-cell transcriptomes reveal heterogeneity of high-grade serous ovarian carcinoma. Clin Transl Med. 2021 Aug;11(8):e500. doi: 10.1002/ctm2.500. PMID: 34459128; PMCID: PMC8335963.

[14] Jang JS, Holicky E, Lau J, McDonough S, Mutawe M, Koster MJ, Warrington KJ, Cuninngham JM. Application of the 3' mRNA-Seq using unique molecular identifiers in highly degraded RNA derived from formalin-fixed, paraffin-embedded tissue. BMC Genomics. 2021 Oct 24;22(1):759. doi: 10.1186/s12864-021-08068-1. PMID: 34689749; PMCID: PMC8543821.

[15] Daniel S. Kermany, Michael Goldbaum, Wenjia Cai, Carolina C.S. Valentim, Huiying Liang, Sally L. Baxter, Alex McKeown, Ge Yang, Xiaokang Wu, Fangbing Yan, Justin Dong, Made K. Prasadha, Jacqueline Pei, Magdalene Y.L. Ting, Jie Zhu, Christina Li, Sierra Hewett, Jason Dong, Ian Ziyar, Alexander Shi, Runze Zhang, Lianghong Zheng, Rui Hou, William Shi, Xin Fu, Yaou Duan, Viet A.N. Huu, Cindy Wen, Edward D. Zhang, Charlotte L. Zhang, Oulan Li, Xiaobo Wang, Michael A. Singer, Xiaodong Sun, Jie Xu, Ali Tafreshi, M. Anthony Lewis, Huimin Xia, Kang Zhang, Identifying Medical Diagnoses and Treatable Diseases by Image-Based Deep Learning, Cell, Volume 172, Issue 5, 2018, Pages 1122-1131.e9,ISSN 0092-8674, https://doi.org/10.1016/j.cell.2018.02.010.

[16] Pectasides D, Pectasides M, Economopoulos T. Brain metastases from epithelial ovarian cancer: a review of the literature. Oncologist. 2006 Mar;11(3):252-60. doi: 10.1634/theoncologist.11-3-252. PMID: 16549809.

[17] Limon D, Shachar E, Wolf I, Adar L, Peleg Hasson S, Ferro L, Safra T. Brain metastases in patients with ovarian cancer. Acta Oncol. 2022 Jun;61(6):757-763. doi: 10.1080/0284186X.2022.2066985. Epub 2022 Apr 29. PMID: 35485453.

[18] Ratner E, Bala M, Louie-Gao M, Aydin E, Hazard S, Brastianos PK. Increased risk of brain metastases in ovarian cancer patients with BRCA mutations. Gynecol Oncol. 2019 Jun;153(3):568-573. doi: 10.1016/j.ygyno.2019.03.004. Epub 2019 Mar 12. PMID: 30876674.

[19] Kuzbari Z, Bandlamudi C, Loveday C, Garrett A, Mehine M, George A, Hanson H, Snape K, Kulkarni A, Allen S, Jezdic S, Ferrandino R, Westphalen CB, Castro E, Rodon J, Mateo J, Burghel GJ, Berger MF, Mandelker D, Turnbull C. Germline-focused analysis of tumour-detected variants in 49,264 cancer patients: ESMO Precision Medicine Working Group recommendations. Ann Oncol. 2023 Mar;34(3):215-227. doi: 10.1016/j.annonc.2022.12.003. Epub 2022 Dec 16. PMID: 36529447.

[20] Schieving JH, de Vries M, van Vugt JM, Weemaes C, van Deuren M, Nicolai J, Wevers RA, Willemsen MA. Alpha-fetoprotein, a fascinating protein and biomarker in neurology. Eur J Paediatr Neurol. 2014 May;18(3):243-8. doi: 10.1016/j.ejpn.2013.09.003. Epub 2013 Sep 29. PMID: 24120489.

[21] Darlix A, Hirtz C, Mollevi C, Ginestet N, Tiers L, Jacot W, Lehmann S. Serum glial fibrillary acidic protein is a predictor of brain metastases in patients with metastatic breast cancer. Int J Cancer. 2021 Oct 15;149(8):1605-1618. doi: 10.1002/ijc.33724. Epub 2021 Jul 19. PMID: 34196964.

[22] Diao B, Yang P. Comprehensive Analysis of the Expression and Prognosis for Laminin Genes in Ovarian Cancer. Pathol Oncol Res. 2021 Aug 25;27:1609855. doi: 10.3389/pore.2021.1609855. Erratum in: Pathol Oncol Res. 2022 Feb 18;28:1610258. doi: 10.3389/pore.2022.1610258. PMID: 34512203; PMCID: PMC8423899.

[23] Chen Y, Ouyang Y, Li Z, Wang X, Ma J. S100A8 and S100A9 in Cancer. Biochim Biophys Acta Rev Cancer. 2023 May;1878(3):188891. doi: 10.1016/j.bbcan.2023.188891. Epub 2023 Mar 29. PMID: 37001615.

[24] Radner S, Banos C, Bachay G, Li YN, Hunter DD, Brunken WJ, Yee KT. β2 and γ3 laminins are critical cortical basement membrane components: ablation of Lamb2 and Lamc3 genes disrupts cortical lamination and produces dysplasia. Dev Neurobiol. 2013 Mar;73(3):209-29. doi: 10.1002/dneu.22057. Epub 2012 Oct 25. PMID: 22961762.

[25] Biswas AK, Han S, Tai Y, Ma W, Coker C, Quinn SA, Shakri AR, Zhong TJ, Scholze H, Lagos GG, Mela A, Manova-Todorova K, de Stanchina E, Ferrando AA, Mendelsohn C, Canoll P, Yu HA, Paik PK, Saqi A, Shu CA, Kris MG, Massague J, Acharyya S. Targeting S100A9-ALDH1A1-Retinoic Acid Signaling to Suppress Brain Relapse in EGFR-Mutant Lung Cancer. Cancer Discov. 2022 Apr 1;12(4):1002-1021. doi: 10.1158/2159-8290.CD-21-0910. PMID: 35078784; PMCID: PMC8983473.

[26] Fong PC, Yap TA, Boss DS, Carden CP, Mergui-Roelvink M, Gourley C, De Greve J, Lubinski J, Shanley S, Messiou C, A'Hern R, Tutt A, Ashworth A, Stone J, Carmichael J, Schellens JH, de Bono JS, Kaye SB. Poly(ADP)-ribose polymerase inhibition: frequent durable responses in BRCA carrier ovarian cancer correlating with platinum-free interval. J Clin Oncol. 2010 May 20;28(15):2512-9. doi: 10.1200/JCO.2009.26.9589. Epub 2010 Apr 20. PMID: 20406929.

[27] Urgen BM, Topac Y, Ustun FS, Demirayak P, Oguz KK, Kansu T, Saygi S, Ozcelik T, Boyaci H, Doerschner K. Homozygous LAMC3 mutation links to structural and functional changes in visual attention networks. Neuroimage. 2019 Apr 15;190:242-253. doi: 10.1016/j.neuroimage.2018.03.077. Epub 2018 Apr 4. PMID: 29626609.

[28] Norquist B, Wurz KA, Pennil CC, Garcia R, Gross J, Sakai W, Karlan BY, Taniguchi T, Swisher EM. Secondary somatic mutations restoring BRCA1/2 predict chemotherapy resistance in hereditary ovarian carcinomas. J Clin Oncol. 2011 Aug 1;29(22):3008-15. doi: 10.1200/JCO.2010.34.2980. Epub 2011 Jun 27. PMID: 21709188; PMCID: PMC3157963.

[29] Kim S, Han Y, Kim SI, Kim HS, Kim SJ, Song YS. Tumor evolution and chemoresistance in ovarian cancer. NPJ Precis Oncol. 2018 Sep 17;2:20. doi: 10.1038/s41698-018-0063-0. PMID: 30246154; PMCID: PMC6141595.

[30] https://www.ensembl.org/info/docs/tools/vep/index.html

[31] Chakravarty D, Gao J, Phillips SM, Kundra R, Zhang H, Wang J, Rudolph JE, Yaeger R, Soumerai T, Nissan MH, Chang MT, Chandarlapaty S, Traina TA, Paik PK, Ho AL, Hantash FM, Grupe A, Baxi SS, Callahan MK, Snyder A, Chi P, Danila D, Gounder M, Harding JJ, Hellmann MD, Iyer G, Janjigian Y, Kaley T, Levine DA, Lowery M, Omuro A, Postow MA, Rathkopf D, Shoushtari AN, Shukla N, Voss M, Paraiso E, Zehir A, Berger MF, Taylor BS, Saltz LB, Riely GJ, Ladanyi M, Hyman DM, Baselga J, Sabbatini P, Solit DB, Schultz

N. OncoKB: A Precision Oncology Knowledge Base. JCO Precis Oncol. 2017 Jul;2017:PO.17.00011. doi: 10.1200/PO.17.00011. Epub 2017 May 16. PMID: 28890946; PMCID: PMC5586540.

[32] Karczewski KJ, Francioli LC, Tiao G, Cummings BB, Alföldi J, Wang Q, Collins RL, Laricchia KM, Ganna A, Birnbaum DP, Gauthier LD, Brand H, Solomonson M, Watts NA, Rhodes D, Singer-Berk M, England EM, Seaby EG, Kosmicki JA, Walters RK, Tashman K, Farjoun Y, Banks E, Poterba T, Wang A, Seed C, Whiffin N, Chong JX, Samocha KE, Pierce-Hoffman E, Zappala Z, O'Donnell-Luria AH, Minikel EV, Weisburd B, Lek M, Ware JS, Vittal C, Armean IM, Bergelson L, Cibulskis K, Connolly KM, Covarrubias M, Donnelly S, Ferriera S, Gabriel S, Gentry J, Gupta N, Jeandet T, Kaplan D, Llanwarne C, Munshi R, Novod S, Petrillo N, Roazen D, Ruano-Rubio V, Saltzman A, Schleicher M, Soto J, Tibbetts K, Tolonen C, Wade G, Talkowski ME; Genome Aggregation Database Consortium; Neale BM, Daly MJ, MacArthur DG. The mutational constraint spectrum quantified from variation in 141,456 humans. Nature. 2020 May;581(7809):434-443. doi: 10.1038/s41586-020-2308-7. Epub 2020 May 27. Erratum in: Nature. 2021 Feb;590(7846):E53. doi: 10.1038/s41586-020-03174-8. Erratum in: Nature. 2021 Sep;597(7874):E3-E4. doi: 10.1038/s41586-021-03758-y. PMID: 32461654; PMCID: PMC7334197.

[33] Gillis S, Roth A. PyClone-VI: scalable inference of clonal population structures using whole genome data. BMC Bioinformatics. 2020 Dec 10;21(1):571. doi: 10.1186/s12859-020-03919-2. PMID: 33302872; PMCID: PMC7730797.

[34] Dang HX, White BS, Foltz SM, Miller CA, Luo J, Fields RC, Maher CA. ClonEvol: clonal ordering and visualization in cancer sequencing. Ann Oncol. 2017 Dec 1;28(12):3076-3082. doi: 10.1093/annonc/mdx517. PMID: 28950321; PMCID: PMC5834020.

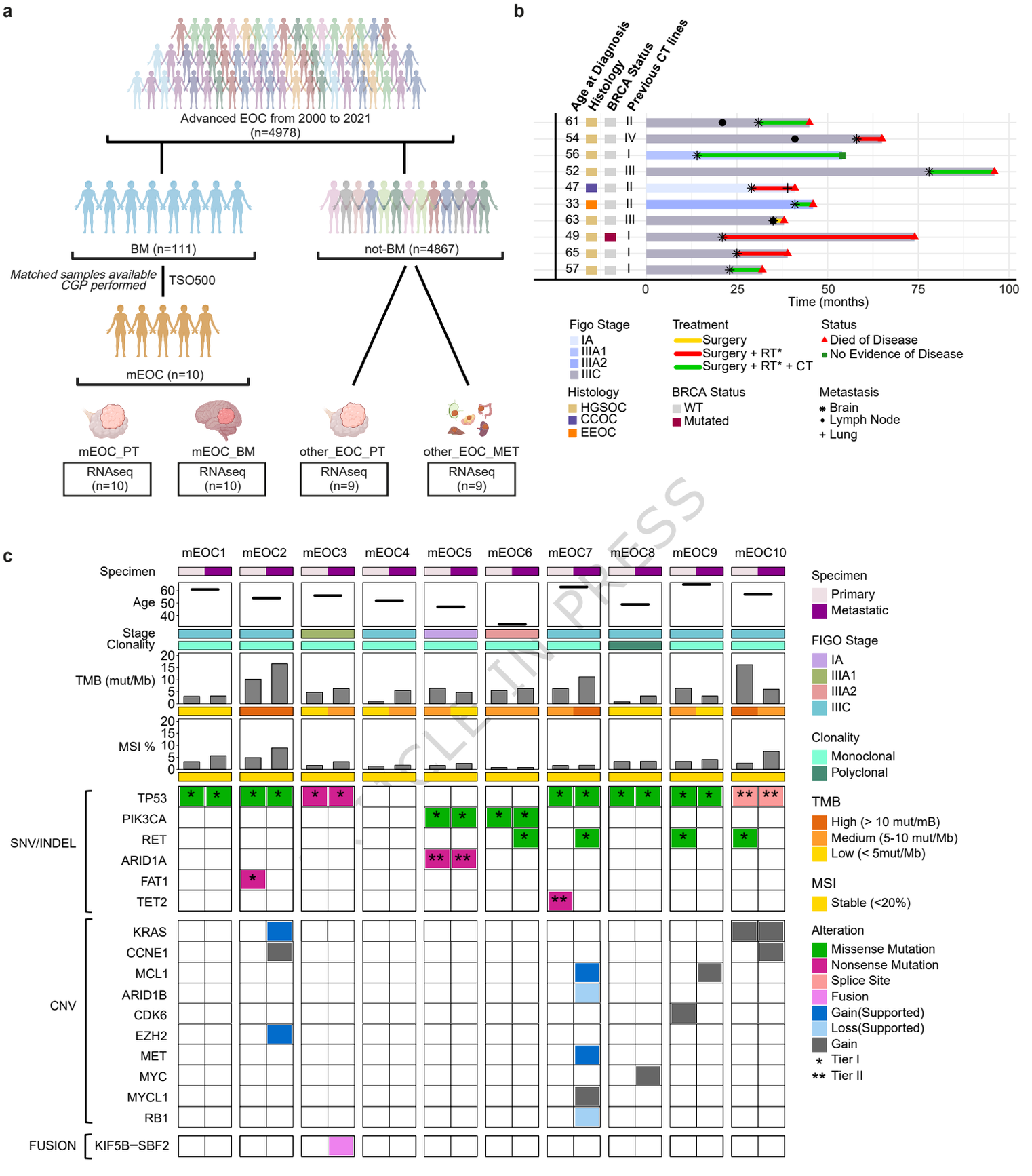

Figure 1

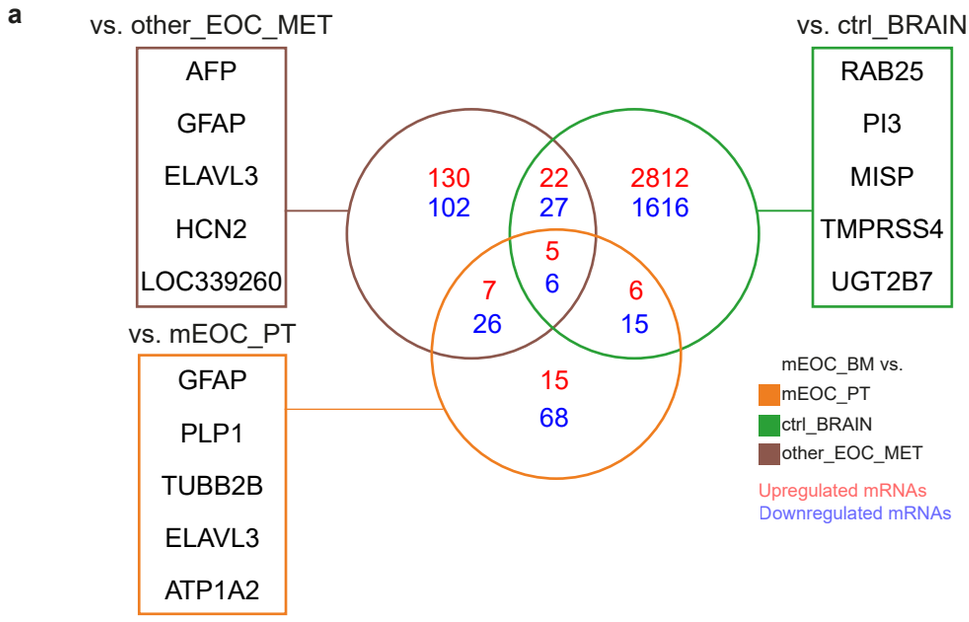

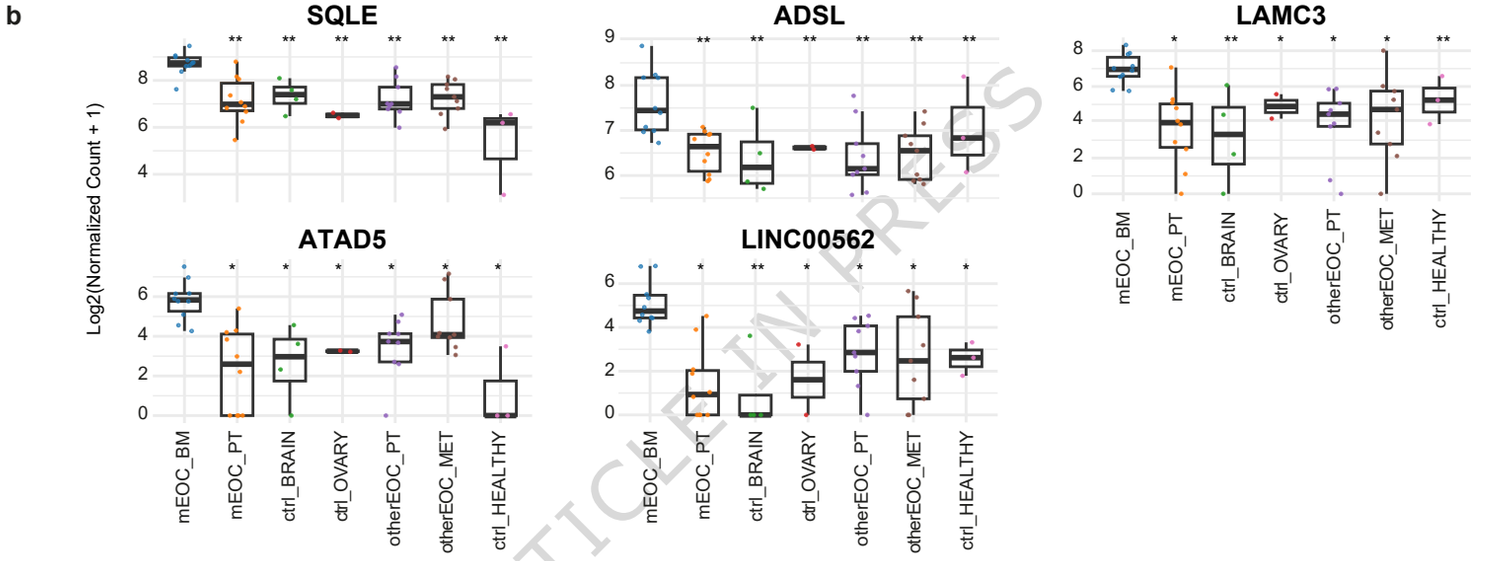

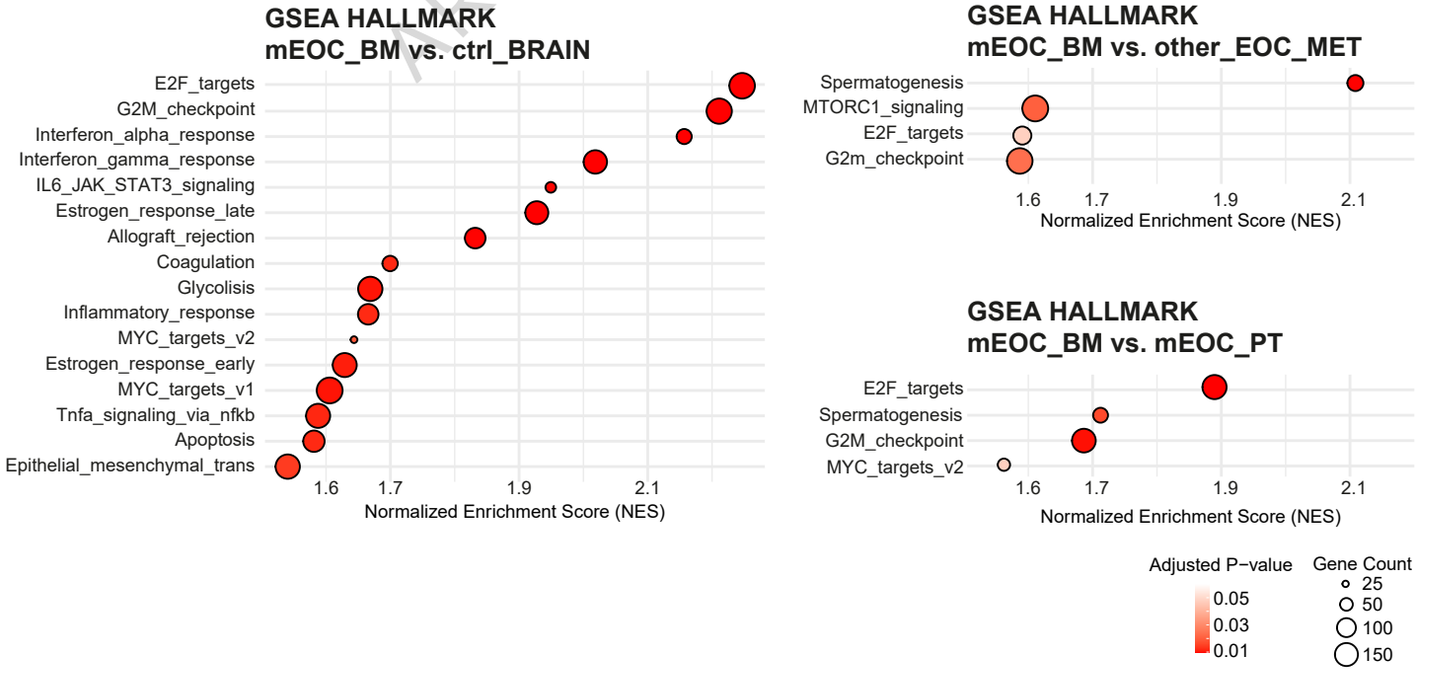

Figure 2

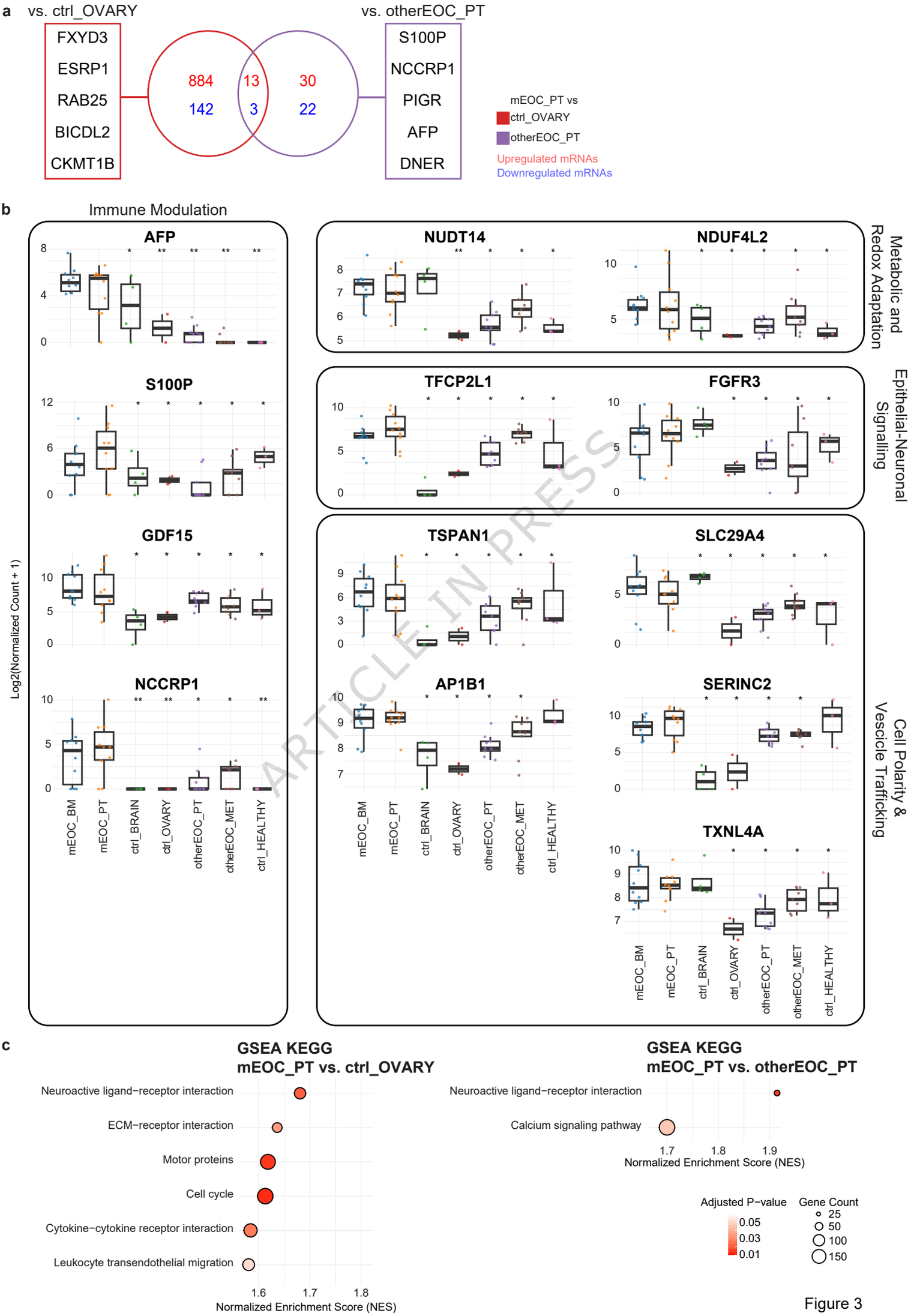

Figure 3

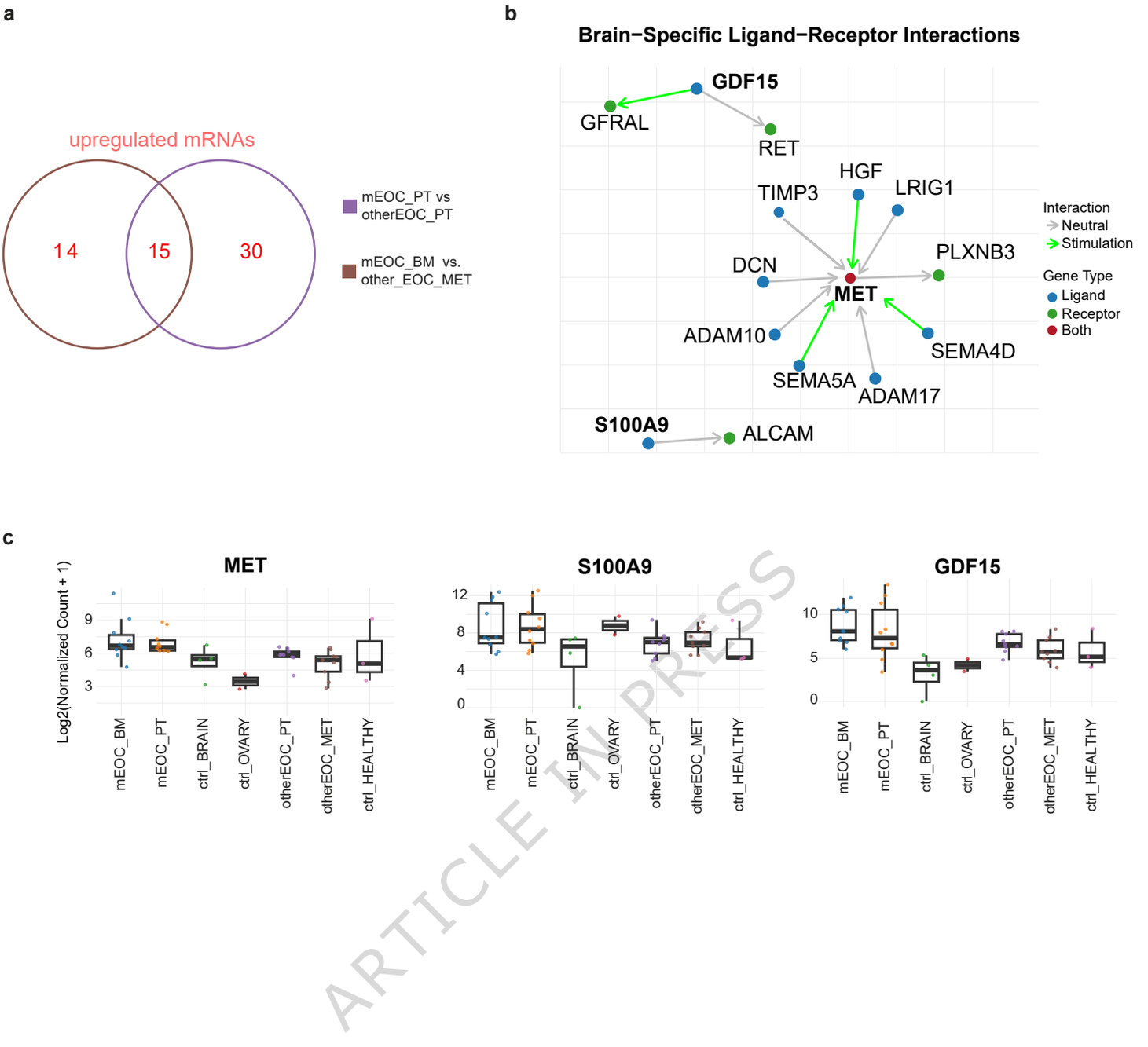

Figure 4